Article

Not peer-reviewed version

Synthesis, Characterization, and Genotoxic and Cytotoxic In Vitro Evaluation of Ceramic Nanoparticles of SC Oxide Powders and Aerogels Doped with Europium

Israel D. Cabrera Rios , Felipe de J. Carrillo Romo * , Antonieta García Murillo , Isela Álvarez González , Eduardo Madrigal Bujaidar

Posted Date: 4 February 2026

doi: 10.20944/preprints202602.0327.v1

Keywords: sol-gel; rare earth; cytokinesis block micronucleus in vitro; genotoxicity; cytotoxicity

Article

Synthesis, Characterization, and Genotoxic and Cytotoxic In Vitro Evaluation of Ceramic Nanoparticles of Sc Oxide Powders and Aerogels Doped with Europium Ion

Isarel D. Cabrera Rios [1], Felipe de J. Carrillo Romo [1,*], Antonieta García Murillo [1], Isela Álvarez González [2] and Eduardo Madrigal Bujaidar [2]

[1] Instituto Politécnico Nacional CIITEC, Cerrada de Cecati s/n; Azcapotzalco, Santa Catarina, Ciudad de Mexico 02250 México

[2] Instituto Politécnico Nacional, Laboratorio de Genética, Escuela Nacional de Ciencias Biológicas, Av. Wilfrido Massieu s/n, Zacatenco, Ciudad de Mexico 07738, México

* Correspondence: fcarrillo@ipn.mx

Abstract

This article reports on the synthesis and characterization of the properties of ceramic powders and aerogels of rare earths using the Sc_2O_3:Eu_2O_3 system synthesized through the sol-gel method, as well as on the toxicological effects of the cytokinesis–block micronucleus cytome assay (CBMC). A variant of the sol-gel method, employing epoxide-assisted gelling and supercritical CO_2 drying, was used to obtain the aerogels. In vitro CBMC assays were employed to assess the genotoxic and cytotoxic effects of the materials' dosages and inherent properties. The morphology of the powders and aerogels consisted of agglomerates of irregularly shaped particles. At the same time, structural analysis revealed crystal sizes of 16 and 10 nm, respectively, for the ceramic powders and aerogels, in which microplastic deformations were observed. The cubic crystalline structure of the Sc_2O_3:Eu_2O_3 system remained unchanged. However, applying "CBMC" and observing the genotoxic and cytotoxic effects of the nanoparticles revealed that the main genotoxic xenobiotic agent was the aerogel. The primary mode of cellular death was necrosis, suggesting that reactive oxygen species might have been involved in the genotoxic and cytotoxic damage.

Keywords: sol-gel; rare earth; cytokinesis block micronucleus in vitro; genotoxicity; cytotoxicity

1. Introduction

The synthesis of engineered materials with particles smaller than 100 nm is advancing the development of new materials with unique properties in both theoretical and applied science, which are performing exceptionally in various fields, including energy development, environmental science, biomedicine, and many others[1,2]. As a result, multiple approaches have been employed to enhance the synthesis of new materials, with the sol-gel process proving to be one of the most suitable methods for obtaining numerous products [3]. Notably, aerogels are valued for their attractive properties, including a high specific surface area, high porosity, and low thermal conductivity.

Rare earths are prized for their unique properties, the versatility, and their suitability for a great number of high- tech applications, due to the electronic configuration and their ability to enhance energy transfer between systems as well as to act as catalysts or sensitizers. The development of new materials based on rare earths allows applications in several fields of applied science.

 doi:10.20944/preprints202602.0327.v1

This approach is worth exploring in-depth. Aerogels made of rare-earth elements can be put to many uses in the high-tech industries and, as a result, are in high demand as unique materials that combine macroscopic external and nanoscale internal structures[4–7]. Nevertheless, the synthesis and characterization of aerogels incorporating a rare-earth matrix remain relatively novel, leaving a significant knowledge gap regarding these materials and their properties, particularly for lanthanide oxide aerogels. Furthermore, the available reports on lanthanide aerogels are confined to the use of alkoxides, chlorides, and nitrates as precursors [8].

However, this represents an opportunity to report for the first time on the properties of ceramic powders and aerogels with a rare earth matrix of scandium oxide, which exhibit exceptional physical and chemical properties, such as the high thermal stability, low electrical conductivity, resistance to corrosion, and a cubic crystalline structure suitable for use in advanced high-tech materials [9]. This work marks the beginning of an in-depth study of the properties of ceramic powders and aerogels, including the genotoxic and cytotoxic effects of nanoparticles interacting with biomolecules, and their biocompatibility and bioactivity. The urgency arises from the increasing, unregulated use of new materials like these and the need to ensure their safety for human and environmental exposure[10–12].

The toxicological potential of a nanoparticle is determined by evaluating its behavior when it is in contact with biological systems and by gauging the inherent hazards of the type of particle[13–16]. Hence, to assess the potential genotoxic and cytotoxic effects of rare- earth nanoparticles currently in use or in the synthesis process, assays that can help deepen our understanding of possible hazards are called for.

The CBMC assay enables the detection of genotoxic and cytotoxic events by comparing DNA damage rates among cells based on the frequency of formation of micronuclei (MNi), nucleoplasmic bridges (NPBs), and nuclear buds (NBUDs), especially in cells that have completed nuclear division. This can lead to an understanding of the mechanism of action of teratogenic agents and the damage they can cause to DNA or chromosomes at points of mutation and the understanding of other forms of genetic damage that result from cellular alterations.

Thus, this paper aims to contribute to current knowledge by evaluating two types of particles in cultured human lymphocytes through use of the CBMC. This method makes possible the study of several parameters associated with DNA or chromosomal damage and an evaluation of preclinical security, a consideration that highlights its potential use in the biomedical field.

2. Results and Discussion

2.1. Microstructure

Figure 1 shows the X-ray diffraction (XDR) patterns of the ceramic powders and aerogels used in the microstructure analysis. The system was well crystallized at 700°C and presents a cubic-centered face structure. The main diffraction peak on plane (222) at 2θ =31.43° of the cubic phase of Sc_2O_3 for each sample, which is consistent with the location of the peaks on the crystallographic chart at CSD 01-088-2159 and CSD 01-086-2476. The addition of the europium oxide (Eu_2O_3) started to form twins. The addition of the europium oxide (Eu_2O_3) started to form twins. In **Figure 1a,** twins formed on all the samples on planes (222) and (440) planes, while in **Figure 1b,** the twins formed only on the sample with the 30% concentration, on plane (222).

 doi:10.20944/preprints202602.0327.v1

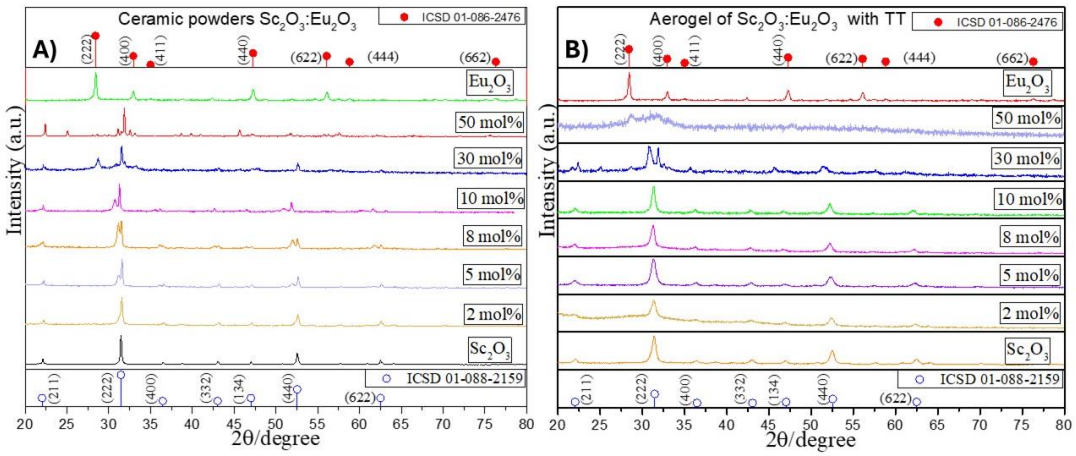

Figure 1. XDR diffractograms of (a) the ceramic powders and (b) the aerogels of the Sc_2O_3: Eu_2O_3 system, presenting the crystallographic planes and the formation of twins corresponding to changes in the concentration of europium oxide.

The formation of twins in the samples indicates plastic microdeformation of the crystal structure and phase changes or phase mixtures [17]. In the ceramic powders in **Figure 1a,** the addition of the Eu^{3+} ion to the matrix enhances the formation of twins not only on the principal peak on plane (222) but also produced twins in the secondary plane (440) starting from a concentration of 5%, which may also be related to slips and the movement of dislocations and the formation of a mixture of phases between them, and the led to formation of a mixture of phases between which were oriented at a particular angle.

The phase mixture was examined by determining the crystallite behavior of the samples. The Scherrer equation (**equation 1**) was used to estimate the sizes at different concentrations.

$$D = \frac{K\lambda}{\beta cos\theta} \quad (1)$$

Figure 2 shows the tendency of crystal growth as the Eu^{3+} ion changes. The tendency, ranging from 17 to 37 nm, is not linear. As noted above, in the diffractograms of the aerogels in **Figure 1b** all the samples present crystallographic planes at (211), (222), (440), and (622) located at 22°, 31°, 52°, 62°, respectively, except for the 30 % concentration of Eu^{3+} ion. Here un contrast plane (622) disappears and presents the formation of a twin oriented at the 30.78 and 31.91 angles, presenting and stretching on the yield by a high charges of compression load, the 50% concentration presents a semi crystalline behavior, featuring a peak that started to form on the on the principal plane (222) of the europium oxide, placed at a 28.62 degree angle, which indicates the beginning of a matrix inversion between the scandium and the europium oxide. **Figure 3** presents the crystal growth tendency of aerogels. In contrast to the powders, the aerogels present a linear decreasing tendency of size, ranging from 12 to 3 nm.

 doi:10.20944/preprints202602.0327.v1

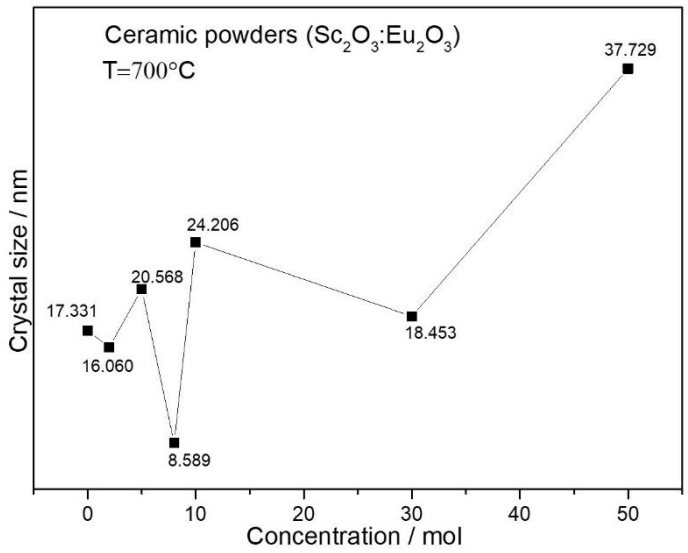

Figure 2. Crystal size versus concentration of ceramics powders of the Sc_2O_3: Eu_2O_3 system reflecting the changing phases resulting from the formation of twins due to microplastic deformation at the grain limit, due in turn to compressive stress charges on the crystalline structure.

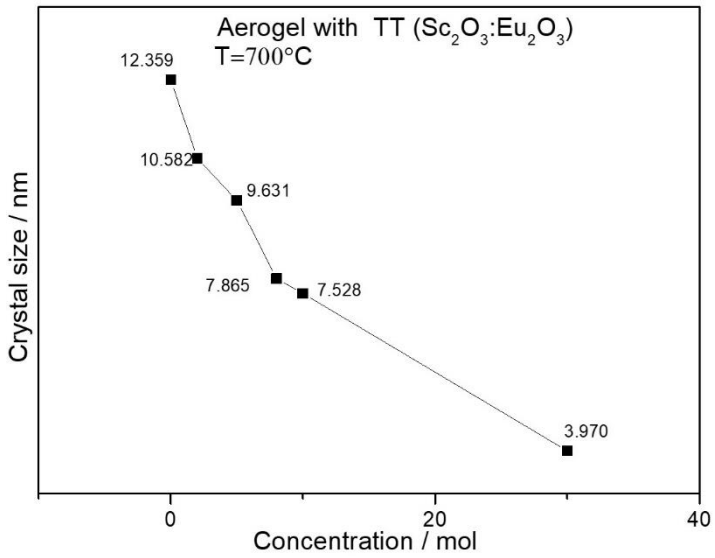

Figure 3. Crystal size versus the concentration of aerogels of the Sc_2O_3: Eu_2O_3 system the linear tendency, and the crystal sizes, can be attributed to supercritical drying and the absence of microplastic deformations.

Distortions on grain boundaries assign all these plastic deformations. However, the formation of twins can be attributed to compressive loads induced by the drying method or heat treatment, which can also cause slips along grain boundaries. This results in a highly compressed elastic yield that can exhibit an asymmetrical reverse stress, a main result of deformation at grain boundaries and partial Shockley dislocations[18–20].

2.1. Morphology

For the morphological analysis, scanning electron microscopy (SEM) and transmission electron microscopy (TEM) were employed to investigate the nanostructure of the powders and aerogels at concentrations of 100% and 2% mol of Eu^{3+}. Figure 4 presents micrographs at 30,000x magnification. **Figures 4a and 4b** display the micrographs of ceramic powders at 100% and 2% concentrations, while **Figure 4c** presents micrographs of the aerogels at the 2% concentration. Qualitatively, both materials

 doi:10.20944/preprints202602.0327.v1

exhibit clusters of quasi-amorphous, interconnected granular particles with random distributions and sizes.

The particle size of the samples were 32.43 nm and 35.85 nm, corresponding to the 100% and 2% concentrations, respectively. The aerogel exhibited a particle size of 45.12 nm. **Figure 4d** displays images from the TEM analysis, showing the morphology of a sample of ceramic powders containing 8% europium ion, illustrating the effects of the increasing ion concentration on morphology. Moreover, the analysis indicated that incorporating higher ion concentrations did not alter the crystal structure or the morphology, as shown in these micrographs.

These analyses are in keeping with the reported dominant planes in the crystal structure, revealing interplanar distances of 2.89, 3.04, and 3.12 nm and aligning with earlier findings. The distances of 2.89 and 3.12 nm align with the main peak on the (222) plane for the oxides Sc and Eu, respectively, as shown in the crystallographic charts, while the 3.04 nm distance is associated with the (220) plane of Sc [9].

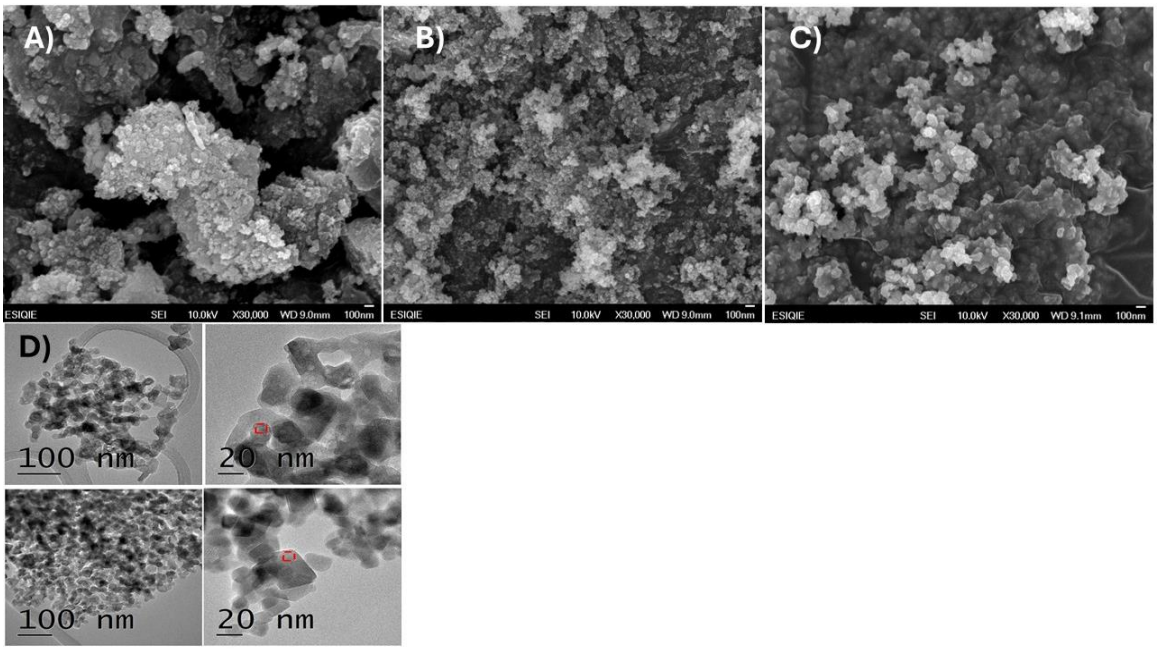

Figure 4. High resolution SEM images of the particles of Sc_2O_3: Eu_2O_3 studied at (30,000x) (a-b) ceramics powders at 100% and 2 % concentration; (c) aerogels at the 2 % concentration; (d) high resolution TEM images of the ceramic powders at the 2% concentration, showing a morphology similar to that seen in the SEM images.

2.2. Cytokinesis Block Micronucleus Assay (CBMC)

The toxicological assessment of the ceramic powders and aerogels included cytogenetic assays using CBMC, following Fenech's criteria [21]. **Table 1** outlines the concentrations, with ceramic powder represented (T1) and the aerogels (T2). This study used mitomycin C as the standard xenobiotic to compare healthy cells with those treated with T1 and T2.

Table 1. Experimental groups used in the cytogenetic assays of the Sc_2O_3: Eu_2O_3 system (where T1 and T2 represent the ceramic powders and the aerogels, respectively), and the concentrations used for the CBMC assay.

Experimental groups	T1 (ceramic powders) Sc_2O_3: Eu_2O_3 (2%)	T2 (aerogels) Sc_2O_3: Eu_2O_3(2%)
Negative control	SSF (1.38µL)	SSF (1.38µL)
Positive control	MC (400µg mL^{-1})	MC (400µg mL^{-1})
Concentration 1	1µg mL^{-1}	1µg mL^{-1}

 doi:10.20944/preprints202602.0327.v1

Concentration 2	0.1µg mL^{-1}	0.1µg mL^{-1}
Concentration 3	0.01µg mL^{-1}	0.01µg mL^{-1}

SSF: physiology saline solution, MC: mitomycin C

The study investigated the in vitro formation of chromosomal damage, possibly induced by nanoparticles, using peripheral blood lymphocytes. This examination could be expanded by scoring additional biomarkers, such as micronuclei, nucleoplasmic bridges, nuclear buds, and necrotic and/or apoptotic cells, thereby providing further insights into DNA damage and its repair, cytostasis, genotoxicity, and cytotoxicity [22–24].

In regard to the cytostasis parameter for thetoxicology characterization, e**quation 2** was used to determine the nuclear division index (NDI);

$$\text{NDI} = \frac{1(\text{mononucleated cells}) + 2\ (\text{binucleated cells}) + 3(\text{multinucleated cells})}{1000\ \text{total de cells}} \quad (2)$$

Figure 5 demonstrates that the impact of the particles on cellular proliferation was not significant, compared to that of the positive control, which contained the antineoplastic agent mitomycin C. Instead, all the cells treated with T1 and T2 presented values comparable to the negative control's NDI of 1.593, demonstrating that the particles had no negative effect on cell division [25,26].

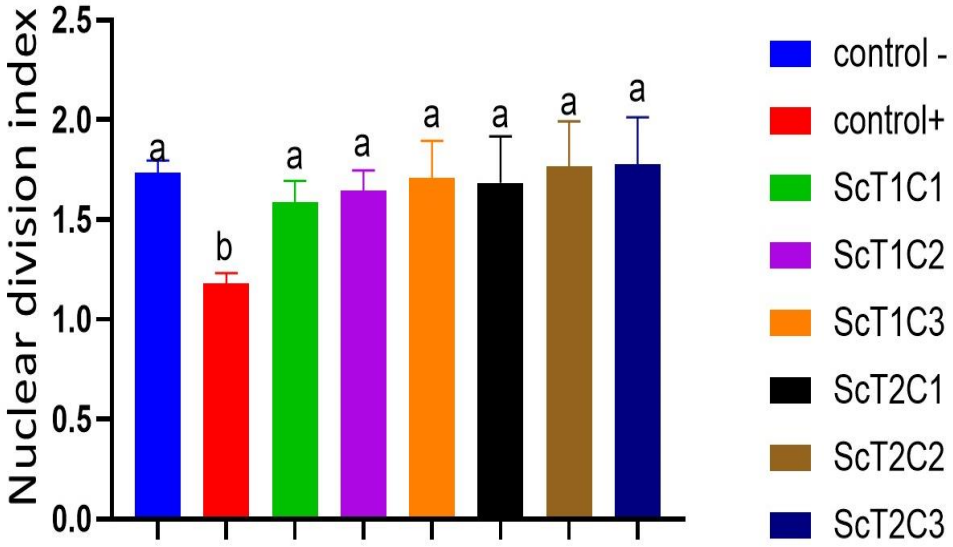

Figure 5. Cytostasis determination of the nanoparticles of Sc_2O_3: Eu_2O_3, where the ceramic powders (T1) and the aerogels (T2) represent the ± 1000 donor cells IDN/treatment/concentration. The letters "a" and "b" indicate statistically significant differences. A one-way analysis if variance (ANOVA) and Tukey test ($p \leq 0.05$) were used to determine statistically significant differences among the samples.

2.2.1. Genotoxicity

As for the genotoxic parameter, **Figure 6a** displays the micronuclei (MNi) results, indicating the formation frequency. Initially, the negative control showed a total of 25 cells with MNi, which aligns with the parameters established by Fenech. In contrast, the samples with positive control present a value of 80 cells with MNi, confirming the genotoxicity of the antineoplastic.

 doi:10.20944/preprints202602.0327.v1

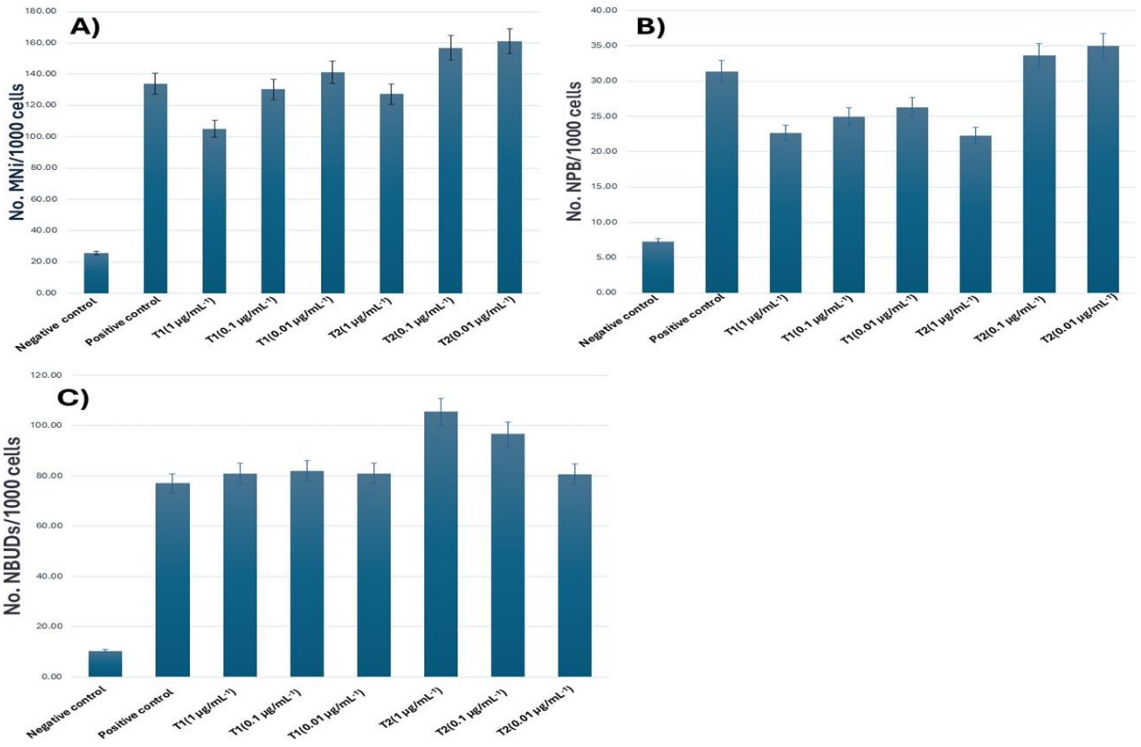

Figure 6. Genotoxic determination parameters (a) micronuclei (MNi); (b) nuclei with plasmic bridges (NBP); (c) nuclear blebs (NBUDs) obtained from ± 1000 binucleated donor cells/treatment/concentration. A one-way ANOVA $p \leq 0.05$ was performed.

In comparison with the positive control, T1 showed no significant increase in concentrations at 1 and 0.1 µg mL^{-1} compared to 0.01 µg mL^{-1}, indicating a 5% increase in formation; for T2, at a concentration of 1 µg mL^{-1}, the behavior was the same as T1; however, this differed for the 0.1 and 0.01 µg mL^{-1} concentrations, which increased formation between 17% and 20%. This indicates a genotoxic effect arising from errors produced during cellular replication, such as segregation or chromosomal breaks, which led to the incorrect incorporation of genetic material [22,27].

Figure 6b illustrates the parameters of nucleoplasmic bridges (NPBs). The negative control exhibits a value of 7 out of 1,000 cells, in contrast to the positive control, which produced a total of 31 cells. For of T1, the generation of NPB did not surpass that of the positive control at any of its concentrations. Conversely, in the case of T2, the concentrations of 0.1 and 0.01 µg mL^{-1} significantly enhance the number of cells exhibiting NPBs, exceeding those of the positive control. This suggests that, although the aerogels did not adversely affect the internal mechanisms of cell division, they induced damage during cellular replication. This phenomenon arises from the rupture of dicentric chromosomes and the erroneous reincorporation of telomeres, resulting in a cross-linking of DNA strands, which in turn leads to the formation of bridges that hinder the proper separation of the nuclei [24,28].

This reorganization of chromosomal damage may be connected to repair mechanisms aimed at reintroducing genetic material into the compromised mitotic spindle or the phosphodiester DNA structure.

As regards the last genotoxic biomarker, nucleoplasmic blebs (NBUDs), **Figure 6c** shows a 5% increase in proliferation for T1 compared to the positive control. In contrast, for T2, a concentration of 1 µg mL^{-1} leds to a 38% increase compared to both the positive control and T1. However, for the lower concentrations of 0.1 and 0.01 µg mL^{-1}, there was a gradual decrease in the proliferation of nuclear blebs, dropping to 25% at 0.1 µg mL^{-1} and following a downward trend until it reached 5%, similar to the behavior of T1. These results enable an evaluation of the genotoxic damage caused by the nanoparticles by observing gene amplification in nuclei that failed to expel them.

 doi:10.20944/preprints202602.0327.v1

2.2.2. Cytotoxicity

The principal mode of cell death, indicated by the cytotoxicity biomarker shown in **Figure 7,** was necrosis. Starting from the highest concentration to the lowest in T1 and T2, necrotic cells increased 7 times compared with the negative control, reaching 54% of the total cells. For the assay, the cells treated with T1 and T2 presented lower values than the positive control, between 11% and14% of necrotic cell formation. For apoptotic cell formation, T1 showed a significant increase at all concentrations compared to the positive control. T2 at a concentration of 0.1 μg mL^{-1} behaved like the positive control, with minimal differences at the lowest concentrations for both treatments (T1 and T2), increasing to 11% to 20% of the total cell amount compared with the positive control.

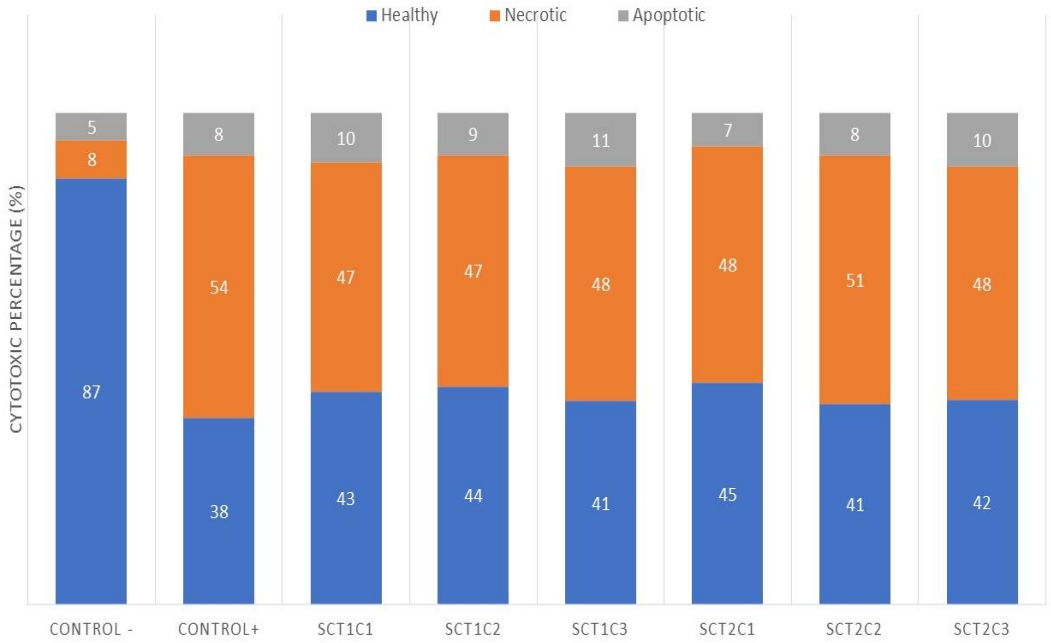

Figure 7. Cytotoxic parameters of necrosis and apoptosis determination of the ± 500 parameter based on the lecturing total of 1000 donor cells/treatment/concentration, expressed as percentages.

Figure 8a shows a photomicrograph of a necrotic cell treated with the scandium particles, showing nuclear condensation, vacuolation, and membrane ruptures. **Figure 8b** displays a cell containing densely packed apoptotic bodies.

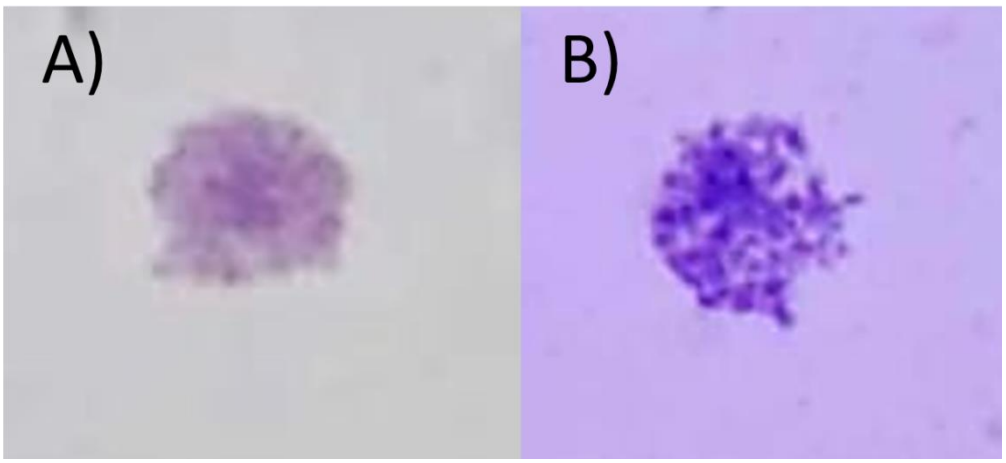

Figure 8. Photomicrographs of (a) necrotic and (b) apoptotic lymphocytes treated with scandium particles at concentrations of 1, 0.1, and 0.01μg/mL^{-1} respectively.

 doi:10.20944/preprints202602.0327.v1

In the case of the T2 samples, the genotoxic behavior for the MNi and NPB parameters is similar, and reducing the concentrations had a greater impact. The effect of the scandium particles is related to the surface principle, which increases the reactivity of particles as their size and, consequently, their surface area is reduced.

A second effect of the scandium particles is their greater electrostatic potential, which, combined with their crystalline structure or interatomic forces of attraction, allows direct interactions among them and enables them to bond with biomolecules, such as lipids and proteins, or with genetic material, once they are internalized by the cell. [29–31].

Hence, the materials from which the scandium nanoparticles are composed and their intrinsic properties contribute to their cytotoxicity [28], and these factors impact the cell membrane's potential and mitochondrial functions on a molecular level, significantly increasing the production of reactive oxygen species (ROS) [30].

The necrosis may be explained by the interactions between the cell and the nanoparticles, which provoke oxidative stress due to ROS, disrupt the normal reduction states in the cellular tissues, and provoke a toxic effect by generating peroxides and free radicals, as the principal cause of deteriorative damage in the cell is direct attacks on DNA, proteins, or lipids (including mitochondrial lipids). This induces cell death through inflammation, karyolysis, vacuolation, or lysis, followed by the release of cellular contents following from the damage [11,32,33].

The necrotic process is a form of cell death that occurs uncontrollably and is not influenced by a specific signaling event, whereas the apoptotic process is induced by the activation of caspase proteases and the fixation of intracellular proteins by caspase-9, which activates the apoptosome complex [34].

In the case of the scandium nanoparticles, the number of healthy cells was lower than the necrotic cells as is stated on **Figure 7,** which the exposure of scandium nanoparticles to the cells also targeted cellular tissues that activate pro-apoptotic factors, releasing of cytochrome C into the cytosol, initiating the contraction of cellular organelles, the condensation of the nuclei, and finally rupturing the packaging of the organelles and fragmenting the cell.

3. Conclusion

Engineered nanomaterials like ceramic powders and aerogels of rare earths present a novel opportunity to explore the toxicology of genotoxic and cytotoxic behaviors in cells and the effects these materials can achieve[31,34,35]. These effects relate to properties such as electronegativity charge, which modulates interactions with biomolecules and constituents; particle sizes (distributions, crystallites); morphology; and even surface area. Such properties lead to increased interactions with cells and facilitate the internalization of particles into cellular membranes where they can compromise vital cell functions [33], and precipitate. Genotoxic and cytotoxic damage during the replication of genetic material.

The structural analysis in this study revealed an average crystal size of 16 nm for T1 and 10 nm for T2. This difference in size is particularly significant because aerogels are known to be mesoporous materials with a large surface area. The morphological and structural properties are highly relevant; the results for T2 in this study demonstrate that not only the administered dose but also the type of nanoparticles is essential when investigating the genotoxicity and cytotoxicity of a material.

Furthermore, it is important to explore how engineered nanomaterials, in their interaction with biomolecules, can evolve and transform to enhance bioavailability by forming biomolecular crowns that significantly influence the reactivity of nanoparticles during their interactions with cells.

The nanoparticles used in this study show promise for applications in a variety of areas. Investigating the genotoxic and cytotoxic behavior of nanoparticles is essential for gaining deeper insights into how they interact with biomolecules and various media. These insights can contribute to the development of new applications and expand our knowledge across different fields.

 doi:10.20944/preprints202602.0327.v1

4. Materials and Methods

4.1. Materials

Scandium oxide (Sc_2O_3, Aldrich, 99.9%), europium oxide (Eu_2O_3, Aldrich, 99.9%), propylene oxide (C_3H_6O, Aldrich, ≥99%), absolute ethyl alcohol (CH_3CH_2OH, Fermont, 99.9%), monohydrate citric acid ($C_6H_8O_7$, Avantor- J.T. Baker, 99%), hydrochloric acid (HCl), physiological saline solution, culture medium RPMI1640, phytohemagglutinin M (Gibco), mitomycin C ($C_{15}H_{18}N_4O_5$, Aldrich), cytochalasin β ($C_{29}H_{37}NO_5$, Aldrich) and potassium chloride (KCl, J.T. Baker) were used in this study.

4.2. Aerogel Synthesis Method

The raw material was synthesized using the epoxide-assisted gelling variant of the sol-gel method[8,36]. First 0.1 g of scandium oxide was combined with europium oxide in several concentrations (Sc: Eu = 100:0, 98:2, 92:8, 90:10, 70:30, and 50:50), then 1ml of hydrochloric acid (HCl) was added, and the mixture was kept under constant agitation until the metal oxide was transformed into a metallic salt, as seen in **Equation 3**.

$$Sc_2O_3 + 6HCl \rightarrow 2ScCl_3 + 3H_2O \quad (3)$$

Once this solution was obtained, the solvent was added with vigorous stirring to ensure complete homogenization and formation of the sol. Subsequently, epoxide and chelating agents were added under vigorous agitation to obtain alcoholics gels, followed by heat treatment at 700°C for 24 h. Finally, supercritical drying was applied at a pressure of 74 bars, as the ceramic powders and the aerogels were subjected to heat treatment at a temperature of 35 °C, which yielded the aerogel.

4.3. Testing Strategy

After synthesizing the products, their structural and morphological properties, and DNA damage, were characterized using XDR to determine the crystalline structure and the sizes of the crystallite of the particles and the influence that they have on their properties, SEM and TEM to determine the morphology, the shape of the surface structures and interplanar distances of the particles, for cytogenetic tests for the toxicology of NPs. The lymphocyte cytokinesis–block micronucleus cytome assay (CBMC) was employed as an in vitro measure of chromosome breaks, following the Fenech methodology [37–40], to evaluate the genotoxic and cytotoxic actions of the particles on the cells.

Abbreviations

The following abbreviations are used in this manuscript:

CBMC	Cytokinesis–block micronucleus cytome assay
MNi	Micronuclei
NPBs	Nucleoplasmic bridges
NBUDs	Nuclear buds
XDR	X-ray diffraction
SEM	Scanning electron microscopy
TEM	Transmission electron microscopy
T1	Ceramic powder treatment
T2	Aerogel treatment
NDI	Nuclear division index
ROS	Reactive oxygen species
HCl	Hydrochloric acid

References

1. E. R. Bandala and M. Berli, "Engineered nanomaterials (ENMs) and their role at the nexus of Food, Energy, and Water," *Mater. Sci. Energy Technol.*, vol. 2, no. 1, pp. 29–40, 2019, doi: 10.1016/j.mset.2018.09.004.

 doi:10.20944/preprints202602.0327.v1

2. S. Bayda, M. Adeel, T. Tuccinardi, M. Cordani, and F. Rizzolio, "The History of Nanoscience and Nanotechnology: From Chemical–Physical Applications to Nanomedicine," *Molecules*, vol. 25, no. Figure 1, pp. 1–15, 2020.
3. A. K. Mishra, "Sol-gel based nanoceramic materials: Preparation, properties and applications," *Sol-gel Based Nanoceramic Mater. Prep. Prop. Appl.*, pp. 1–297, 2016, doi: 10.1007/978-3-319-49512-5.
4. M. Aegerter, N. Leventis, and M. Koebel, Aerogels handbook (Advances in Sol-Gel Derived Materials and Technologies). 2011.
5. I. Smirnova and P. Gurikov, "Aerogel production: Current status, research directions, and future opportunities," *J. Supercrit. Fluids*, vol. 134, no. December 2017, pp. 228–233, 2018, doi: 10.1016/j.supflu.2017.12.037.
6. A. Benad *et al.*, "Mechanical Properties of Metal Oxide Aerogels," *Chem. Mater.*, vol. 30, no. 1, pp. 145–152, 2018, doi: 10.1021/acs.chemmater.7b03911.
7. M. K. Hossain *et al.*, "A review on recent applications and future prospects of rare earth oxides in corrosion and thermal barrier coatings, catalysts, tribological, and environmental sectors," *Ceram. Int.*, vol. 48, no. 22, pp. 32588–32612, 2022, doi: 10.1016/j.ceramint.2022.07.220.
8. W. Chu *et al.*, "Rare earth lanthanum based aerogels with reduced chlorine ions by a modified epoxide gelation method," *Chem. Phys. Lett.*, vol. 761, no. October, p. 138072, 2020, doi: 10.1016/j.cplett.2020.138072.
9. C. Zhang, Z. Zhou, Z. Tang, D. Ballo, C. Wang, and G. Jian, "Effects of scandium oxide on domain structure, dielectric and ferroelectric properties of barium zirconate titanate ceramics," *J. Alloys Compd.*, vol. 889, p. 161622, 2022, doi: 10.1016/j.jallcom.2021.161622.
10. M. A. Saifi, W. Khan, and C. Godugu, "Cytotoxicity of Nanomaterials: Using Nanotoxicology to Address the Safety Concerns of Nanoparticles," *Pharm. Nanotechnol.*, vol. 6, no. 1, pp. 3–16, 2018, doi: 10.2174/2211738505666171023152928.
11. Y. Niu and M. Tang, "In vitro review of nanoparticles attacking macrophages: Interaction and cell death," *Life Sci.*, vol. 307, no. July, p. 120840, 2022, doi: 10.1016/j.lfs.2022.120840.
12. J. G. Keller *et al.*, "Aerogels are not regulated as nanomaterials, but can be assessed by tiered testing and grouping strategies for nanomaterials," *Nanoscale Adv.*, vol. 3, no. 13, pp. 3881–3893, 2021, doi: 10.1039/d1na00044f.
13. M. Secu, C. Secu, and C. Bartha, "Optical Properties of Transparent Rare-Earth Doped Sol-Gel Derived Nano-Glass Ceramics," *Materials (Basel).*, vol. 14, no. 6871, 2021, doi: doi.org/10.3390/ma14226871 Academic.
14. M. A. Worsley *et al.*, "Chlorine-free, monolithic lanthanide series rare earth oxide aerogels via epoxide-assisted sol-gel method," *J. Sol-Gel Sci. Technol.*, vol. 89, no. 1, pp. 176–188, 2018, doi: 10.1007/s10971-018-4811-y.
15. B. Marcus A . Worsley, Hayward; Alexander E . Gash, "MONOLITHIC RARE EARTH OXIDE AEROGELS," vol. 2, pp. 1–7, 2019.
16. M. Parashar, V. K. Shukla, and R. Singh, "Metal oxides nanoparticles via sol–gel method: a review on synthesis, characterization and applications," *J. Mater. Sci. Mater. Electron.*, vol. 31, no. 5, pp. 3729–3749, 2020, doi: 10.1007/s10854-020-02994-8.
17. Z. Pei, S. Zhang, Y. Lei, F. Zhang, and M. Chen, "Decoupling between Shockley partials and stacking faults strengthens multiprincipal element alloys," *Proc. Natl. Acad. Sci. U. S. A.*, vol. 118, no. 51, pp. 1–6, 2021, doi: 10.1073/pnas.2114167118.
18. J. Zhou, J. Shen, F. A. Essa, and J. Yu, "Twins and grain boundaries-dominated the reverse Bauschinger effect and tension-compression asymmetry," *J. Mater. Res. Technol.*, vol. 18, pp. 15–28, 2022, doi: 10.1016/j.jmrt.2022.02.080.
19. S. Zhao, Y. Xu, X. Lin, C. Geng, Y. Lian, and Y. Dong, "The activation of compression twin pairs and plasticity improvement of directionally solidified Mg alloy," *J. Mater. Res. Technol.*, vol. 18, pp. 461–469, 2022, doi: 10.1016/j.jmrt.2022.02.066.
20. Q. Li *et al.*, "Effect of scandium addition on microstructure and mechanical properties of as-cast Al-5%Cu alloys," *Vacuum*, vol. 177, no. April, p. 109385, 2020, doi: 10.1016/j.vacuum.2020.109385.

21. M. Fenech, "Cytokinesis-block micronucleus cytome assay," *Nat. Protoc.*, vol. 2, no. 5, pp. 1084–1104, 2007, doi: 10.1038/nprot.2007.77.
22. OECD, "Test No. 487: In Vitro Mammalian Cell Micronucleus Test, OECD Guidelines for the Testing of Chemicals, Section 4," no. 487, 2023, [Online]. Available: https://doi.org/10.1787/9789264264861-en
23. M. Fenech *et al.*, "Molecular mechanisms of micronucleus, nucleoplasmic bridge and nuclear bud formation in mammalian and human cells," *Mutagenesis*, vol. 26, no. 1, pp. 125–132, 2011, doi: 10.1093/mutage/geq052.
24. V. Gubala *et al.*, "Engineered nanomaterials and human health: Part 1. Preparation, functionalization and characterization (IUPAC Technical Report)," *Pure Appl. Chem.*, vol. 90, no. 8, pp. 1283–1324, 2018, doi: 10.1515/pac-2017-0101.
25. T. D. Pollard and B. O'Shaughnessy, "Molecular mechanism of cytokinesis," *Annu. Rev. Biochem.*, vol. 88, pp. 661–689, 2019, doi: 10.1146/annurev-biochem-062917-012530.
26. T. A. Qiu, P. L. Clement, and C. L. Haynes, "Linking nanomaterial properties to biological outcomes: analytical chemistry challenges in nanotoxicology for the next decade," *Chem. Commun.*, vol. 54, no. 91, pp. 12787–12803, 2018, doi: 10.1039/c8cc06473c.
27. A. A. Sousa, P. Schuck, and S. A. Hassan, "Biomolecular interactions of ultrasmall metallic nanoparticles and nanoclusters," *Nanoscale Adv.*, vol. 3, no. 11, pp. 2995–3027, 2021, doi: 10.1039/d1na00086a.
28. M. Repetto Jiménez and G. Kuhn Repetto, *Toxicología Fundamental*, 4th ed. España, 2024.
29. M. S. D'Arcy, "Cell death: a review of the major forms of apoptosis, necrosis and autophagy," *Cell Biol. Int.*, vol. 43, no. 6, pp. 582–592, 2019, doi: 10.1002/cbin.11137.
30. A. Erofeev *et al.*, "Novel method for rapid toxicity screening of magnetic nanoparticles," *Sci. Rep.*, vol. 8, no. 1, pp. 1–11, 2018, doi: 10.1038/s41598-018-25852-4.
31. D. Laha, R. Grant, P. Mishra, and N. Nilubol, "The Role of Tumor Necrosis Factor in Manipulating the Immunological Response of Tumor Microenvironment," *Front. Immunol.*, vol. 12, no. April, pp. 1–12, 2021, doi: 10.3389/fimmu.2021.656908.
32. F. Villanueva-Flores, A. Castro-Lugo, O. T. Ramírez, and L. A. Palomares, "Understanding cellular interactions with nanomaterials: Towards a rational design of medical nanodevices," *Nanotechnology*, vol. 31, no. 13, 2020, doi: 10.1088/1361-6528/ab5bc8.
33. A. C. Sabuncu, J. Grubbs, S. Qian, T. M. Abdel-Fattah, M. W. Stacey, and A. Beskok, "Probing nanoparticle interactions in cell culture media," *Colloids Surfaces B Biointerfaces*, vol. 95, pp. 96–102, 2012, doi: 10.1016/j.colsurfb.2012.02.022.
34. J. D. Webster and D. Vucic, "The Balance of TNF Mediated Pathways Regulates Inflammatory Cell Death Signaling in Healthy and Diseased Tissues," *Front. Cell Dev. Biol.*, vol. 8, no. May, pp. 1–14, 2020, doi: 10.3389/fcell.2020.00365.
35. S. Murugadoss *et al.*, "Agglomeration of titanium dioxide nanoparticles increases toxicological responses in vitro and in vivo," *Part. Fibre Toxicol.*, vol. 17, no. 1, pp. 1–14, 2020, doi: 10.1186/s12989-020-00341-7.
36. M. Fenech, "The in vitro micronucleus technique," *Mutat. Res. - Fundam. Mol. Mech. Mutagen.*, vol. 455, no. 1–2, pp. 81–95, 2000, doi: 10.1016/S0027-5107(00)00065-8.
37. S. Sommer, I. Buraczewska, and M. Kruszewski, "Micronucleus assay: The state of art, and future directions," *Int. J. Mol. Sci.*, vol. 21, no. 4, pp. 7–9, 2020, doi: 10.3390/ijms21041534.
38. M. A. Rodrigues, L. A. Beaton-Green, R. C. Wilkins, and M. F. Fenech, "The potential for complete automated scoring of the cytokinesis block micronucleus cytome assay using imaging flow cytometry," *Mutat. Res. - Genet. Toxicol. Environ. Mutagen.*, vol. 836, pp. 53–64, 2018, doi: 10.1016/j.mrgentox.2018.05.003.
39. M. Fenech, "Cytokinesis-block micronucleus cytome assay evolution into a more comprehensive method to measure chromosomal instability," *Genes (Basel).*, vol. 11, no. 10, pp. 1–13, 2020, doi: 10.3390/genes11101203.
40. M. Fenech, W. P. Chang, M. Kirsch-Volders, N. Holland, S. Bonassi, and E. Zeiger, "HUMN project: Detailed description of the scoring criteria for the cytokinesis-block micronucleus assay using isolated human lymphocyte cultures," *Mutat. Res. - Genet. Toxicol. Environ. Mutagen.*, vol. 534, no. 1–2, pp. 65–75, 2003, doi: 10.1016/S1383-5718(02)00249-8.

 doi:10.20944/preprints202602.0327.v1